Self-Lifting Droplet Driven by the Solidification-Induced Solutal Marangoni Flow

Feng Wang, Li Chen, Yuqi Li, Peng Huo, Xi Gu, Man Hu, and Daosheng Deng*
Department of Aeronautics and Astronautics, Fudan University, Shanghai 200433, China

(Received 12 October 2023; accepted 6 December 2023; published 2 January 2024)

Multicomponent droplets are pertinent to diverse applications ranging from 3D printing to fabrication of electronic devices to medical diagnostics and are typically inherent with the occurrence of the phase transition in the manifestation of evaporation and solidification. Indeed, the versatile transformations and fascinating morphologies of the droplets have been identified, which primarily arise from the evaporation-induced flow. Here, we report the self-lifting behavior of a frozen binary droplet, resulting in a nearly doubling in height, in a fashion that defies against the gravitational effect. This counterintuitive observation is attributed to an internal solutal Marangoni flow up to 1 mm/s, which is driven by the enriched solute concentration locally in the vicinity of the solidification front. Moreover, we perform theoretical analysis by incorporating the propagation of solidification front, and the calculated spatiotemporal evolution of droplet shape agrees with experiments excellently. The effects of several key physical parameters on self-lifting are elucidated quantitatively, providing guidance to control the self-lifting. These results will further advance our understanding of underlying physicochemical hydrodynamics in the multicomponent liquid systems subjected to heat transfer and phase change, consequently shedding light on the relevant technological applications.

DOI: 10.1103/PhysRevLett.132.014002

Multicomponent droplets consisting of more than one liquid component [1–3] are indispensable for diverse applications, including 3D printing [4,5], fabrication of electronic devices [6], and medical diagnostics [7]. Since being inherent with the rich physicochemical hydrodynamics, multicomponent droplets are typically characterized by the occurrence of the phase transition in the manifestation of evaporation and solidification [1]. Particularly, the evaporation at the air-liquid interface of the droplets has been extensively investigated recently. This evaporation generates the gradient of the solute concentration and the gradient of surface tension, and the internal flow accordingly leads to the intriguing dynamics and exotic phenomena. For example, in a volatile colloidal droplet, an outward capillary flow carries dispersed particles, which accumulate toward the pinned contact line, and deposits them into a line to form the residual coffee rings [8]. The evaporation-induced Marangoni flow within a binary-mixture liquid droplet is strong enough to generate a micron-thick pancakelike shape [9]. Because of selective evaporation and the density gradient, the flow within droplets is effectively controlled by the gravitational effect [10]; a protein-containing droplet experiences the shape morphing to a flattened and wrinkled encapsulated state due to the gravity and evaporation [11].

Concurrently, the study of frozen droplets undergoing supercooling has been emerging [12]. Since the advancing solidification front is immanent in phase change, heat transfer, and mass transport, generating an intimate interaction with the dispersed objects submerged within the liquid, many fascinating behaviors can appear. For example, a water droplet on a supercooling substrate will form an ice-cone shape associated with the geometry of the freezing front as determined by heat transfer [13]. For an oil-in-water emulsion during freezing process, the increased solute concentration at the solidification front can enhance premelting for the engulfment of droplets [14], and the droplet can be formed into a pointy-tip shape as mediated by nanometer-thick interfacial flows [15]. Despite the significant progresses of evaporation-induced solutal Marangoni flow for the multicomponent liquid, the effects of solidification on the probable flow and shape transformation in the multicomponent liquids have been less investigated.

In this Letter, by utilizing the high-speed imaging and thermal imaging, we observe a counterintuitive self-lifting behavior for a water-ethanol binary droplet subjected to supercooling, resulting in a nearly doubling in height, in a fashion that defies the gravitational effect. This phenomenon is attributed to an internal solidification-induced solutal Marangoni flow, which deforms the shape to be elevated upward. A theoretical model agrees with the experiments remarkably, and the effects of several key physical parameters on the self-lifting are elucidated quantitatively. These results would inspire more future research to explore solidification-induced flow for the relevant technological applications.

Observation of the self-lifting behavior.—A binary ethanol-water droplet (the initial volume concentration of ethanol c_0) was gently deposited on a supercooled surface (the substrate temperature T_s), and the freezing dynamics is sketched in Fig. 1(a) (Supplemental Material [16], Note 1).

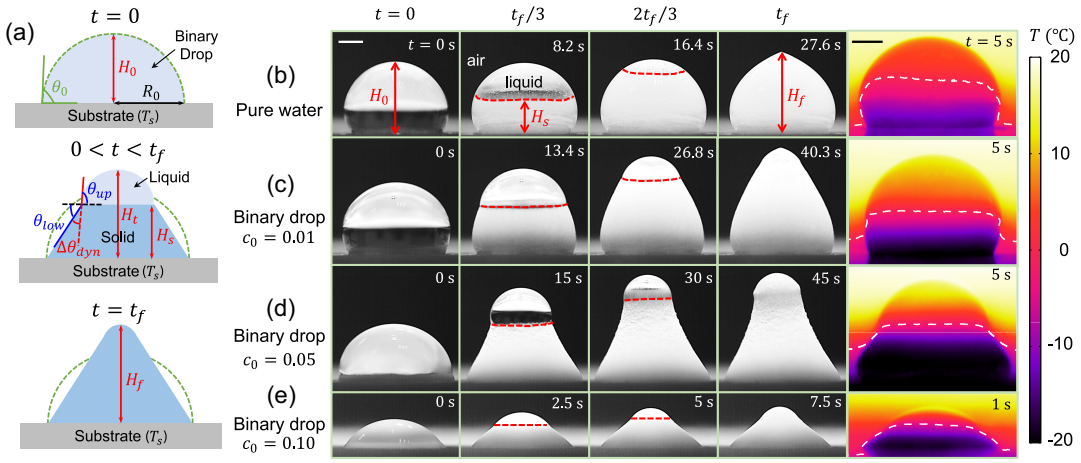

FIG. 1. Self-lifting of a frozen binary droplet on a supercooled surface. (a) Sketch for a frozen binary droplet for the initial state ($t = 0$), the self-lifting state ($0 < t < t_f$), and the final state ($t = t_f$), respectively. H_0, R_0, θ_0 for the initial height, radius, and apparent contact angle of the binary droplet; H_t, H_s, H_f for the time-dependent total height, the height of the solidification front, and the final height of the frozen binary droplet; θ_{low}, θ_{up}, and $\Delta\theta_{\text{dyn}}$ for the contact angle at the solid-gas interface, liquid-gas interface, and the dynamic growth angle. High-speed imaging and thermal imaging snapshots for (b) pure water droplet $c_0 = 0$, $T_s = -23.5\,^{\circ}\text{C}$; (c) binary droplet $c_0 = 0.01$, $T_s = -22.5\,^{\circ}\text{C}$; (d) binary droplet $c_0 = 0.05$, $T_s = -21.5\,^{\circ}\text{C}$; (e) binary droplet $c_0 = 0.10$, $T_s = -20.1\,^{\circ}\text{C}$. The red dashed line for the solidification front in high-speed images, and the white dashed line for the isotherm $T = T_f$ (for the freezing point of the binary liquid) in thermal images. Scale bar for 1 mm.

By utilizing high-speed camera and thermal camera, the spatiotemporal evolution of the freezing dynamics was recorded at various ethanol concentrations [Figs. 1(b)–1(e), Supplemental Material, Movie S1–4). For a pure water droplet [Fig. 1(b)], during the whole freezing process from $t = 0$ to t_f, the transition between the solid-gas interface and the liquid-gas interface at the solidification front is so smooth that the initial droplet profile is nearly preserved in the final frozen shape, although the volume expansion causes a sharp tip at the apex of the droplet [13].

However, for a binary droplet [Figs. 1(c)–1(e)], the interface transition at the solidification front is so sharp that the different contact angles at the solid-gas interface (θ_{low}) and the liquid-gas interface (θ_{up}) form a pronounced dynamic growth angle ($\Delta\theta_{\text{dyn}}$), as indicated in the sketch of Fig. 1(a) [17]. The top residual droplet above the solidification front undergoes deformation and lifting up. Eventually at t_f, the final height of a frozen binary droplet (H_f) is much greater than the initial height (H_0).

From the high-speed imaging, the total height (H_t) of the droplet as a function of time is obtained, as shown in Fig. 2(a), and the final self-lifting behavior as characterized by a dimensionless height ratio, H_f/H_0, has a nonmonotonic relation with the concentration c_0, and reaches a peak at a medium concentration ($c_0 = 0.05$) [Fig. 2(b)]. Since the surface tension of the ethanol-water binary mixture decreases with ethanol concentration c_0 (Supplemental Material, Note 2), the initial apparent contact angle of the binary droplet θ_0 on the supercooled surface is expected to decrease with c_0 accordingly, consistent with the experiments [Fig. 2(c)].

Propagation of solidification front.—In order to understand the freezing dynamics of a binary droplet, the solidification front is simplified to be flat hereafter [dashed lines in Figs. 1(c)–1(e)]. By considering the balance between the latent heat released at the solidification front and the heat transfer across the solid, the height of solidification front (H_s) grows with time as follows [13,18]:

$$H_s = 2\sqrt{D_s t}, \tag{1}$$

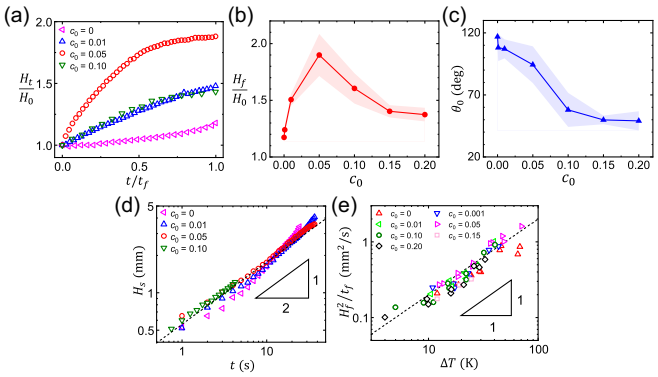

FIG. 2. Dynamics of self-lifting for a binary droplet. (a) The time evolution of self-lifting ratio H_t/H_0 at different c_0. (b) The final self-lifting ratio H_f/H_0 of a binary droplet at different c_0. (c) The initial apparent contact angle θ_0 of a binary droplet at different c_0. (d) The propagation of the solidification front with a $1/2$ scaling law at different c_0. (e) The effective diffusivity of the solidification front ($H_f^2/t_f = 4D_s$) linearly proportional to ΔT, but independent of c_0. The shadow in (b) and (c) for the standard deviation of at least five measurements.

where $D_s = 2k_s\Delta T/(\rho_s L)$ is a diffusion coefficient, k_s, ρ_s are the thermal conductivity and the density of the solidified liquid, respectively; L is the latent heat of solidification per unit mass; $\Delta T = T_f - T_s$ is the supercooling temperature, and T_f is concentration-dependent freezing point of the binary droplet (Supplemental Material, Note 2).

The propagation of the solidification front [Fig. 2(d)] still can be well described by this $1/2$ scaling law for the ice front propagation in a pure liquid. Additionally, this scaling law is experimentally validated by the effective diffusivity $H_f^2/t_f = 4D_s \sim \Delta T$ at different supercooling temperatures ΔT, while being independent of ethanol concentration c_0, as shown in Fig. 2(e) [18,19].

Solutal Marangoni flow.—For a multicomponent droplet such as a binary ethanol-water droplet investigated here, as shown in the sketch [Fig. 3(a)], during the freezing process, the solute (ethanol) is extruded from the solidification front due to the lower freezing point [14]. By this fashion, the solutal concentration is accumulated locally near the vicinity of the solidification front in the liquid phase, so the solute concentration is enhanced near the solidification front (c_{high}), while the concentration at the top liquid is less (c_{low}). Since the surface tension decreases with ethanol concentration, accordingly the local surface tension at the bottom liquid (γ_{low}) is reduced to be lower than the surface tension at the top liquid (γ_{high}). Consequently, a solutal Marangoni flow is generated within the liquid phase, resulting in an upward solutal Marangoni flow at the droplet interface while a downward flow inside the droplet, as marked by yellow arrows in Fig. 3(a).

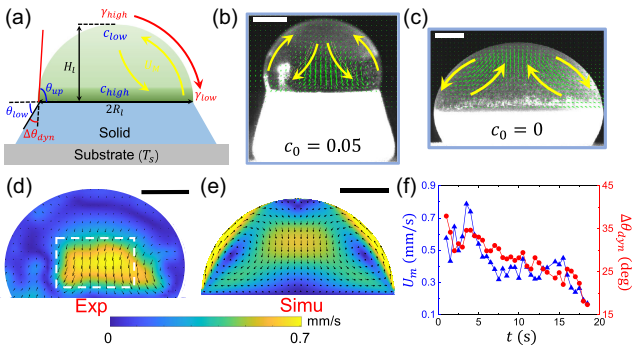

FIG. 3. Solutal Marangoni flow near the vicinity of solidification front in the liquid phase for a frozen binary droplet. (a) Sketch for the self-lifting behavior. θ_{low}, θ_{up}, and $\Delta\theta_{\mathrm{dyn}}$ for the contact angle at the solid-gas interface, liquid-gas interface, and the dynamic growth angle; H_l, R_l for the height and radius of the remaining liquid phase during the droplet freezing; the green shadow for the concentration distribution of ethanol. During the propagation of the solidification front, the solute (ethanol) concentration at the front (c_{high}) is accumulated and enriched, becoming greater than the concentration at the apex (c_{low}). Consequently, the concentration-dependent surface tension (red arrow) generates a solutal Marangoni flow (yellow arrow), forming an upward solutal Marangoni flow U_M along the interface. (b) PIV measurement of a frozen binary droplet, $c_0 = 0.05$, $T_s = -37.8\,^{\circ}\mathrm{C}$. (c) PIV measurement of a frozen water droplet, $c_0 = 0$, $T_s = -33.6\,^{\circ}\mathrm{C}$. (d) Flow field in (b). (e) Solutal Marangoni flow field obtained by simulation. (f) The evolution of U_m and $\Delta\theta_{\mathrm{dyn}}$ obtained from experiments. Scale for 1 mm.

In order to validate the solutal Marangoni flow, particle image velocimetry (PIV) measurement is performed during the freezing process of a binary droplet. Figure 3(b) shows a typical snapshot of flow field in a frozen binary droplet ($c_0 = 0.05$), and a pronounced downward flow field at the center of the droplet is observed. In contrast, the flow field inside a frozen pure water droplet is opposite to the binary case, and this upward flow at the center of the droplet [Fig. 3(c)] arises from the thermal Marangoni effect due to the interfacial temperature gradient [20]. Furthermore, the downward flow pattern at the center of a freezing binary droplet [Fig. 3(d)] is validated by the simulation involving the solutal Marangoni flow due to concentration gradient [Fig. 3(e) and Supplemental Material, Note 3). Also, the simulation presents the flow structure near the interface, which is challenging to be measured accurately for the curved or distorted interface [20].

Because of the existence of the upward solutal Marangoni flow, the profile of droplet differs pronouncedly from the initial profile. The apparent contact angle of the droplet on the ice substrate (θ_{up}) becomes larger than the angle of the ice substrate (θ_{low}), and a dynamic growth angle $\Delta\theta_{dyn} = \theta_{\mathrm{up}} - \theta_{\mathrm{low}}$ is identified (Fig. 3(a)). The typical solutal Marangoni velocity U_m inside a freezing binary droplet is defined as the maximum velocity at the center of the droplet, marked by the white dash box in Fig. 3(d). As shown in Fig. 3(f), both $\Delta\theta_{dyn}$ and U_m decrease with the propagation of the solidification front experimentally.

From the perspective of scaling analysis, by balancing the viscous force with the surface tension gradient [1,9], the typical velocity of the Marangoni flow can be expressed as,

$$U_M \propto \frac{\Delta\gamma(c,T)H_l}{\mu R_l}, \tag{2}$$

where $\Delta\gamma(c,T)$ is the difference of surface tension, which can be induced by a temperature gradient or a concentration gradient, μ is the viscosity of the liquid, H_l and R_l are the height and radius of the remaining droplet in the phase of liquid, respectively.

Additionally, the competition between the thermal Marangoni effect $\Delta\gamma_T$ and the solutal Marangoni effect $\Delta\gamma_c$ can be expressed as follows:

$$\frac{\Delta\gamma_T}{\Delta\gamma_c} \sim \frac{|d\gamma/dT|\cdot(T_0 - T_f)/R_0}{|d\gamma/dc|\cdot c_0/\delta_c}, \tag{3}$$

where $|d\gamma/dT| = 2\times10^{-4}\,\mathrm{N/(m\,K)}$, $|d\gamma/dc| = 0.1\ \mathrm{N/m}$ are the surface tension gradients dependent on temperature

and concentration, respectively. δ_c is the thickness of the concentration boundary layer, which is typically much smaller than the radius of droplet R_0 [14]. Hence, the resultant $\Delta\gamma_T/\Delta\gamma_c \ll 1$ evidently indicates the dominant role of the solutal Marangoni effect in the frozen binary droplet as investigated here.

According to Eq. (2), the decrease of U_m as the solidification front propagates [Fig. 3(f)] may result from the decreased aspect ratio H_l/R_l and the reduced surface tension gradient $d\gamma/dc$ associated with the increased concentration inside the remaining droplet (Supplemental Material, Note 2). This scaling relation of the solutal Marangoni flow U_M [Eq. (2)] is further validated by the simulation (Supplemental Material, Note 3).

Moreover, we explore the self-lifting behavior on an inclined surface with tilt angle $\theta_s = 45°$ (Supplemental Material, Note 4), and the dimensionless time-dependent height of the freezing droplet H_t/H_0 exhibits a similar behavior, implying the negligible gravitational effect and further highlighting the essential role of the solutal Marangoni flow to be responsible for the self-lifting.

Dynamic growth angle.—After understanding the characteristic of the solutal Marangoni flow inside a freezing binary droplet, we further investigate the dynamic growth angle $\Delta\theta_{\mathrm{dyn}}$ at different volume concentration c_0. From the high-speed images [Figs. 1(c)–1(e)], the evolution of the apparent contact angle of the remaining droplet θ_{up} and the ice substrate θ_{low} are extracted at different concentrations c_0 [Figs. 4(a)–4(c)]. Remarkably, despite the complicated evolution of the apparent contact angles during the frozen process, the dynamic growth angle $\Delta\theta_{\mathrm{dyn}}$ is still pronounced [Fig. 4(d)].

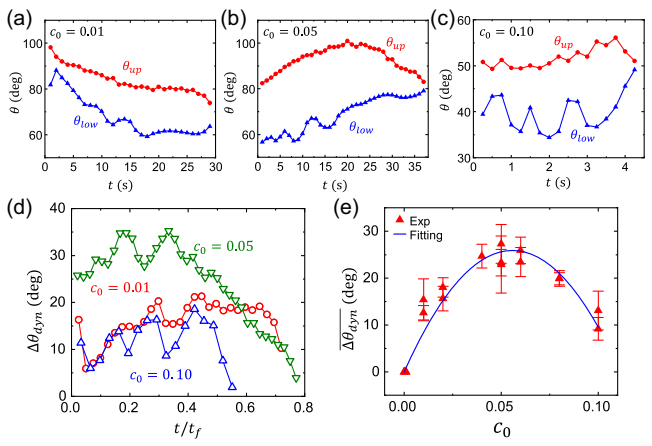

FIG. 4. Dynamic growth angle of a frozen binary droplet. (a)–(c) The evolution of the apparent contact angle of the remaining droplet θ_{up} and the ice substrate θ_{low} at different concentration c_0. (d) Evolution of the dynamic growth angle $\Delta\theta_{\mathrm{dyn}} = \theta_{\mathrm{up}} - \theta_{\mathrm{low}}$ at different c_0. (e) The time-averaged dynamic growth angle $\overline{\Delta\theta_{\mathrm{dyn}}}$ for $t/t_f < 0.5$ in (d) at different c_0, triangles for the experimental results, the solid line for the fitting result to guide the eye, and error bars for the standard deviation of at least five data points.

Figure 4(e) indicates that the time-averaged $\overline{\Delta\theta_{\mathrm{dyn}}}$ reaches a peak at a medium concentration ($c_0 = 0.05$). According to Eq. (2), for a lower concentration ($c_0 < 0.05$), the surface tension difference $\Delta\gamma$ is dominant, which increases with the initial concentration c_0, promoting the solutal Marangoni flow and dynamic growth angle $\Delta\theta_{\mathrm{dyn}}$. On the other hand, for a higher concentration ($c_0 > 0.05$), the aspect ratio H_l/R_l, which is dependent on the initial apparent contact angle θ_0, becomes much smaller with the increased concentration c_0, suppressing the solutal Marangoni flow and $\Delta\theta_{\mathrm{dyn}}$.

Model for self-lifting.—In order to understand the self-lifting behavior quantitatively, we proceed to perform the theoretical calculation for the evolution of the droplet shape during the freezing process. The dynamic growth angle associated with the self-lifting is required to be considered carefully. Actually, a general framework to describe solidification was established by including the dynamic growth angle, which is the angle between the tangents to the solid-vapor and liquid-vapor interfaces at the tri-junction [17,21].

Here, by combining the mass conservation, the propagation of solidification front [Eq. (1)], and the geometrical relation [Fig. 3(a)] (Supplemental Material, Note 5), the contour of a frozen binary droplet can be calculated with the initial profile of the droplet R_0, θ_0, and the constant $\Delta\theta_{\mathrm{dyn}}$ [17,21]. Here, to simplify the model, the dynamic growth angle $\Delta\theta_{\mathrm{dyn}}$ correlated with the solutal Marangoni flow is assumed to be a constant during the freezing process, and its value is obtained from the experiments [Fig. 4(e)].

Remarkably, Fig. 5(a) shows the theoretical calculation of droplet profiles agrees with the experimental observation

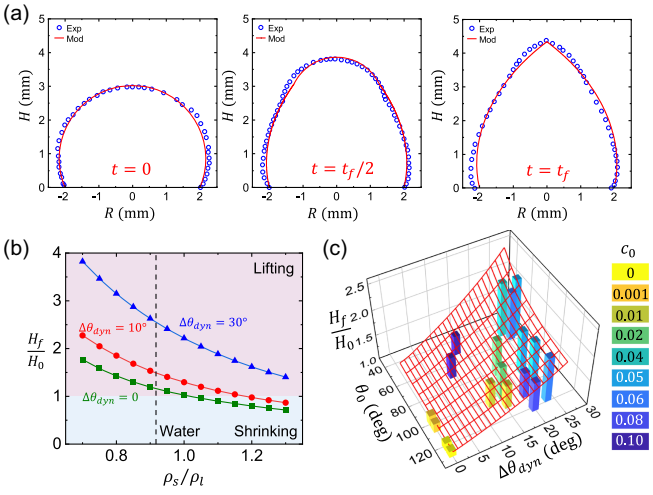

FIG. 5. Theoretical model for the self-lifting behavior. (a) For the spatiotemporal evolution of droplet profile, the numerical model consistent with the experiment [for $c_0 = 0.01$ in Fig. 1(c)]. (b) The calculated self-lifting height ratio, H_f/H_0, dependent on density ratio ρ_s/ρ_l and $\Delta\theta_{\mathrm{dyn}}$ for a given $\theta_0 = 90°$. (c) Calculated H_f/H_0 (transparent curved surface) as a function of initial contact angle (θ_0) and the dynamic growth angle ($\Delta\theta_{\mathrm{dyn}}$) for water $\rho_s/\rho_l = 0.917$; experimentally measured values (bars) and theoretically estimated values exhibit similar trends.

excellently during the solidification process (Supplemental Material, Movie S5). More physical parameters can be examined for the final self-lifting height ratio in the model. Taken as an example, Fig. 5(b) demonstrates the self-lifting height ratio (H_f/H_0) as a function of the ratio of solid and liquid density ratio (ρ_s/ρ_l) for different $\Delta\theta_{\mathrm{dyn}}$. The red and blue regimes denote for the self-lifting ($H_f/H_0 > 1$) and self-shrinking ($H_f/H_0 < 1$). Clearly, for water with $\rho_s/\rho_l = 0.917$, the self-lifting effect becomes much higher at a large $\Delta\theta_{\mathrm{dyn}}$.

From the model calculation, Fig. 5(c) displays the self-lifting ratio H_f/H_0 associated with the initial contact angle (θ_0) and the dynamic growth angle ($\Delta\theta_{\mathrm{dyn}}$). The self-lifting value at different concentrations (c_0), corresponding to (θ_0, $\Delta\theta_{\mathrm{dyn}}$) as observed experimentally, exhibits excellent agreement with calculation.

In conclusion, we report a counterintuitive self-lifting in a frozen binary droplet in a fashion that defies the gravitational effect. This observation is attributed to an internal solutal Marangoni flow, which is driven by the enriched solute concentration locally in the vicinity of the solidification front. We perform theoretical analysis of spatiotemporal evolution of frozen droplet, consistent with experiments excellently. These results will further advance our understanding of the rich physicochemical hydrodynamics in the multicomponent liquid systems subjected to heat transfer and phase change, consequently shedding light on the relevant technological applications for the advanced manufacturing.

We are thankful for the fruitful discussions with Professor H. A. Stone and Professor K. L. Chong. This work is supported by the funding from the National Program in China, start-up in Fudan University, and State Key Laboratory of Airliner Integration Technology and Flight Simulation.

*dsdeng@fudan.edu.cn

[1] D. Lohse and X. H. Zhang, Physicochemical hydrodynamics of droplets out of equilibrium, Nat. Rev. Phys. **2**, 426 (2020).

[2] N. Blanken, M. S. Saleem, M. J. Thoraval, and C. Antonini, Impact of compound drops: A perspective, Curr. Opin. Colloid Interface Sci. **51**, 101389 (2021).

[3] Z. Y. Wang, D. Orejon, Y. Takata, and K. Sefiane, Wetting and evaporation of multicomponent droplets, Phys. Rep. **960**, 1 (2022).

[4] M. Vaezi, H. Seitz, and S. F. Yang, A review on 3D micro-additive manufacturing technologies, Int. J. Adv. Manuf. Technol. **67**, 1721 (2013).

[5] Y. Zhang, Z. C. Dong, C. X. Li, H. F. Du, N. X. Fang, L. Wu, and Y. L. Song, Continuous 3D printing from one single droplet, Nat. Commun. **11**, 4685 (2020).

[6] J. A. Lim, W. H. Lee, H. S. Lee, J. H. Lee, Y. D. Park, and K. Cho, Self-organization of ink-jet-printed triisopropylsilylethynyl pentacene via evaporation-induced flows in a drying droplet, Adv. Funct. Mater. **18**, 229 (2008).

[7] D. Brutin, B. Sobac, B. Loquet, and J. Sampol, Pattern formation in drying drops of blood, J. Fluid Mech. **667**, 85 (2011).

[8] R. D. Deegan, O. Bakajin, T. F. Dupont, G. Huber, S. R. Nagel, and T. A. Witten, Capillary flow as the cause of ring stains from dried liquid drops, Nature (London) **389**, 827 (1997).

[9] A. A. Pahlavan, L. S. Yang, C. D. Bain, and H. A. Stone, Evaporation of binary-mixture liquid droplets: The formation of picoliter pancakelike shapes, Phys. Rev. Lett. **127**, 024501 (2021).

[10] Y. X. Li, C. Diddens, P. Y. Lv, H. Wijshoff, M. Versluis, and D. Lohse, Gravitational effect in evaporating binary microdroplets, Phys. Rev. Lett. **122**, 114501 (2019).

[11] D. Riccobelli, H. H. Al-Terke, P. Laaksonen, P. Metrangolo, A. Paananen, R. H. A. Ras, P. Ciarletta, and D. Vella, Flattened and wrinkled encapsulated droplets: Shape morphing induced by gravity and evaporation, Phys. Rev. Lett. **130**, 218202 (2023).

[12] S. Jung, M. K. Tiwari, N. V. Doan, and D. Poulikakos, Mechanism of supercooled droplet freezing on surfaces, Nat. Commun. **3**, 615 (2012).

[13] A. G. Marin, O. R. Enriquez, P. Brunet, P. Colinet, and J. H. Snoeijer, Universality of tip singularity formation in freezing water drops, Phys. Rev. Lett. **113**, 054301 (2014).

[14] D. Dedovets, C. Monteux, and S. Deville, Five-dimensional imaging of freezing emulsions with solute effects, Science **360**, 303 (2018).

[15] J. G. Meijer, P. Kant, D. Van Buuren, and D. Lohse, Thin-film-mediated deformation of droplet during cryopreservation, Phys. Rev. Lett. **130**, 214002 (2023).

[16] See Supplemental Material at http://link.aps.org/supplemental/10.1103/PhysRevLett.132.014002 for the details of the experimental setup, the liquid properties, the numerical simulation, the dynamic model, and the self-lifting on an inclined surface. Also, see Supplemental Movies 1–6.

[17] D. M. Anderson, M. G. Worster, and S. H. Davis, The case for a dynamic contact angle in containerless solidification, J. Cryst. Growth **163**, 329 (1996).

[18] M. Hu, F. Wang, Q. Tao, L. Chen, S. M. Rubinstein, and D. S. Deng, Frozen patterns of impacted droplets: From conical tips to toroidal shapes, Phys. Rev. Fluids **5**, 081601 (R) (2020).

[19] E. Ghabache, C. Josserand, and T. Séon, Frozen impacted drop: From fragmentation to hierarchical crack patterns, Phys. Rev. Lett. **117**, 074501 (2016).

[20] Linn Karlsson, Henrik Lycksam, Anna-Lena Ljung, Per Gren, and T Staffan Lundström, Experimental study of the internal flow in freezing water droplets on a cold surface, Exp. Fluids **60**, 182 (2019).

[21] H. Zeng, S. J. Lyu, D. Legendre, and C. Sun, Influence of gravity on the freezing dynamics of drops on a solid surface, Phys. Rev. Fluids **7**, 103605 (2022).